

A 100 kpc nebula associated with the “Teacup” fading quasar

M. Villar-Martín^{1,2}, A. Cabrera-Lavers^{3,4}, A. Humphrey⁵, M. Silva⁵

C. Ramos Almeida^{4,6}, J. Piqueras^{1,2}, B. Emons⁷

¹Centro de Astrobiología (CSIC-INTA), Carretera de Ajalvir, km 4, 28850 Torrejón de Ardoz, Madrid, Spain

²Astro-UAM, UAM, Unidad Asociada CSIC, Facultad de Ciencias, Campus de Cantoblanco, E-28049, Madrid, Spain

³GRANTECAN, Cuesta de San José s/n, E-38712, Breña Baja, La Palma, Spain

⁴Instituto de Astrofísica de Canarias, Vía Láctea s/n, E-38200 La Laguna, Tenerife, Spain

⁵Instituto de Astrofísica e Ciências do Espaço, Universidade do Porto, CAUP, Rua das Estrelas, PT4150-762 Porto, Portugal

⁶Departamento de Astrofísica, Universidad de La Laguna (ULL), E-38205 La Laguna, Tenerife, Spain

⁷National Radio Astronomy Observatory, 520 Edgemont Road, Charlottesville, VA 22903, USA

Accepted ?. Received ?; in original form ?.

ABSTRACT

We report the discovery of a ~ 100 kpc ionized nebula associated with the radio quiet type 2 quasar (QSO2) nicknamed the “Teacup” ($z=0.085$). The giant nebula is among the largest known around active galaxies at any z . We propose that it is part of the circumgalactic medium (CGM) of the QSO2 host, which has been populated with tidal debris by galactic interactions. This rich gaseous medium has been rendered visible due to the illumination by the powerful active nucleus (AGN). Subsolar abundances ($\sim 0.5Z_{\odot}$) are tentatively favored by AGN photoionization models. We also report the detection of coronal emission (Fe^{+6}) from the NE bubble, at ~ 9 kpc from the AGN. The detection of coronal lines at such large distances from the AGN and the $[\text{NII}]\lambda 6583/\text{H}\alpha$, $[\text{SII}]\lambda\lambda 6716, 6731/\text{H}\alpha$, $[\text{OI}]\lambda 6300/\text{H}\alpha$ optical emission line ratios of the giant nebula are consistent with the fading quasar scenario proposed by Gagne et al. (2014). The fading rate appears to have been faster in the last $\sim 46,000$ yr. Deep wide field integral field spectroscopy of giant nebulae around powerful AGN such as the “Teacup’s” with instruments such as MUSE on VLT opens up a way to detect and study the elusive material from the CGM around massive active galaxies thanks to the illumination by the luminous AGN.

Key words: galaxies: active - galaxies: evolution - quasars: individual: SDSS J143029.88+133912.0 (the “Teacup”)

1 INTRODUCTION

The “Teacup” (SDSS J143029.88+133912.0 at $z=0.085$) is a radio quiet type 2 quasar (QSO2), whose nickname comes from the peculiar morphology of the extended ionized gas. It shows a loop-shaped emission line structure reminiscent of a “handle” extending up to ~ 12 kpc NE of the active galactic nucleus (AGN) (Keel et al. 2012, Gagne et al. 2014, Ramos Almeida et al. 2017). This object has been subject of an intensive study by different groups for two main reasons. On one hand, the modeling of the emission line spectra with AGN photoionization models has led to the conclusion that it is a fading quasar (Gagne et al. 2014, Keel et al. 2017). The luminosity of the active nucleus appears to have dropped by ~ 2 orders of magnitude in the last $\sim 46,000$ years. On

the other hand, the system has been proposed to be the scenario of a giant outflow generated by an AGN wind or induced by a ~ 1 kpc radio jet whose effects are noticed up to ~ 10 - 12 kpc from the AGN and may be responsible for the bubble-like morphology inspiring its nickname (Harrison et al. 2015). A detailed description of the general properties of the “Teacup” can be found in this paper.

We present here new results based on optical long slit spectroscopic data obtained with the Spanish Gran Telescopio Canarias (GTC). We analyze and interpret the properties (size, kinematics, line ratios) of a newly discovered giant reservoir of ionized gas associated with the “Teacup”, which extends for more than 100 kpc. New results related to the coronal emission from the NE ionized bubble are also presented. The paper is organized as follows: we describe briefly

the observations and data reduction in Sect. 2. Results are presented in Sect. 3 and discussed in Sect. 4 and summarized Sect. 5.

We adopt $H_0=71$ km s⁻¹ Mpc⁻¹, $\Omega_\Lambda=0.73$ and $\Omega_m=0.27$. This gives an arcsec to kpc conversion 1.58 kpc arcsec⁻¹ at $z=0.085$.

2 OBSERVATIONS AND DATA REDUCTION

Long slit spectroscopic observations were performed on February 26th 2017 (programme GTC13-16B) in visitor mode with the optical imager and long slit spectrograph OSIRIS¹ mounted on the 10.4m GTC. The R2500R volume-phased holographic grating (VPH) was used, which provides a spectral coverage of 5575-7685 Å with dispersion 1.04 Å pixel⁻¹. A 1.5 arcsec wide slit was used at two different orientations (Fig. 1): position angle PA 60° (N to E), along the main axis of the NE bubble and PA 0°, in the E-W direction along the South edge of this bubble. The spectral resolution FWHM_{inst} measured from several prominent sky lines is 5.28 ± 0.14 Å (223 ± 6 km s⁻¹ at the the observed H α wavelength). The pixel scale is 0.254 arcsec pixel⁻¹.

Eight 300 sec spectra were obtained at each orientation to complete a total exposure time of 2400 sec per PA. Shifts were applied in the slit direction of 20" between consecutive exposures for both a better fringing correction and a more accurate background subtraction. The seeing FWHM during the observations was 1.4 ± 0.1 arcsec (FWHM), as measured from several stars in the acquisition images. The spectra were reduced and flux calibrated following standard procedures (see Villar Martín et al. 2017 for details).

2.1 Additional data

We have also used two archive HST images of the “Teacup” (program 12525, principal investigator W.C. Keel; Keel et al. 2015). The emission line+continuum image was obtained on June 14th 2012 with the Advanced Camera for Surveys (ACS) and the WFC detector. This provides a pixel scale of 0.05 arcsec pixel⁻¹. The FR716N ramp filter was used, which covers the ~ 6850 - 7470 Å spectral range (~ 6313 - 6885 Å rest frame for the “Teacup”). It thus includes H α + $[\text{NII}]\lambda\lambda 6548,6583$ and $[\text{SII}]\lambda\lambda 6716,6731$ and emission line structures will appear very prominently.

The continuum image was obtained on June 13th 2012 with the Wide Field Camera 3 (WFC3). The F763M medium band filter was used in the UVIS channel, which provides a pixel scale of 0.04 arcsec pixel⁻¹. The filter covers the ~ 7243 - 8036 Å range (~ 6675 - 7406 Å rest frame). The image is dominated by continuum emission. Some non-negligible contribution of lines such as $[\text{SII}]\lambda\lambda 6716,6731$ may be expected in emission line dominated structures.

3 RESULTS

3.1 The giant ionized gas reservoir

We show in Fig. 1 the HST FR716N image of the “Teacup”. Emission line structures such as the ionized bubbles appear very prominently. The two GTC-Osiris slit positions at PA60 and PA90 are over-plotted. The 2D spectra of $[\text{NII}]\lambda\lambda 6548,6583+\text{H}\alpha$ along both PA are also shown with different contrasts to highlight the low and high surface brightness structures. Several features are also identified. G1 (PA60) is an emission line galaxy at $z=0.317$. G2 (PA90) is also a galaxy. The detection of a line at 5851 Å (probably $[\text{OII}]\lambda 3727$) and the tentative detection of another one at ~ 7635 Å (probably H β) suggest G2 is at $z=0.570$.

The 2D spectra of the “Teacup” reveal line emission across giant extensions along both PA. H α is detected up to $R60(max)_{NE} \sim 53$ kpc and $R60(max)_{SW} \sim 58$ kpc to the NE and SW respectively from the continuum centroid along PA60. It extends up to $R90(max)_E \sim 40$ kpc to the E along PA90. Detection is confirmed up to $R90(max)_W \sim 31$ kpc to the W. Fainter H α is tentatively detected up to ~ 63 kpc, although this needs confirmation with deeper data.

We have thus discovered a giant reservoir of gas (>100 kpc total extension) associated with the “Teacup”, which extends far beyond the radio and optical bubbles, each one having radial sizes of ~ 10 - 12 kpc. The long slit and integral field spectroscopic studies of Gagne et al. (2014) and Harrison et al. (2015) already revealed the existence of gas beyond the bubbles. However, due to the shallowness of the data and/or the small field of view of the instruments, emission was confirmed only up to ~ 11 arcsec or 17.4 kpc from the AGN².

We show in Fig. 2 the FR763M HST image. Low surface brightness asymmetric continuum features (tidal tails, shells) are appreciated across several 10s of kpc. They are the remnants of the merger of a small, dynamically cold system with the bulge dominated QSO2 host (Keel et al. 2015). The maximum radial extensions of the H α emission along the long slit spectra are indicated with blue arrows. Despite the incomplete spatial coverage in two spatial dimensions, the huge extension along both PA and the rather symmetric radial sizes at both sides of the AGN suggest that the “Teacup” is embedded in a giant gaseous reservoir. The purple ellipse shows a possible geometry of the nebula, adjusted in angle and size to fit the radial sizes of the H α extension in different directions from the QSO2 along PA60 and PA90. The ionized bubbles are comparatively tiny.

3.1.1 Ionization mechanism

We have extracted two 1D spectra from the highest surface brightness regions of the nebula along PA60, beyond the NE bubble (Fig. 1). Aperture 1 (Ap. 1) is centered at 11.5 arcsec (18.2 kpc) from the QSO2 continuum centroid and is 4.8 arcsec wide (7.6 kpc). The G1 galaxy is within this aperture, but no emission line contamination is expected by it because the redshift $z=0.317$ is very different. Aperture 2

² The comparison of Gagne et al. (2014) velocity curve along PA95 in their Fig. 8 with our own data leads us to conclude that their spatial axis is in pixels instead of arcsec.

¹ <http://www.gtc.iac.es/en/pages/instrumentation/osiris.php>

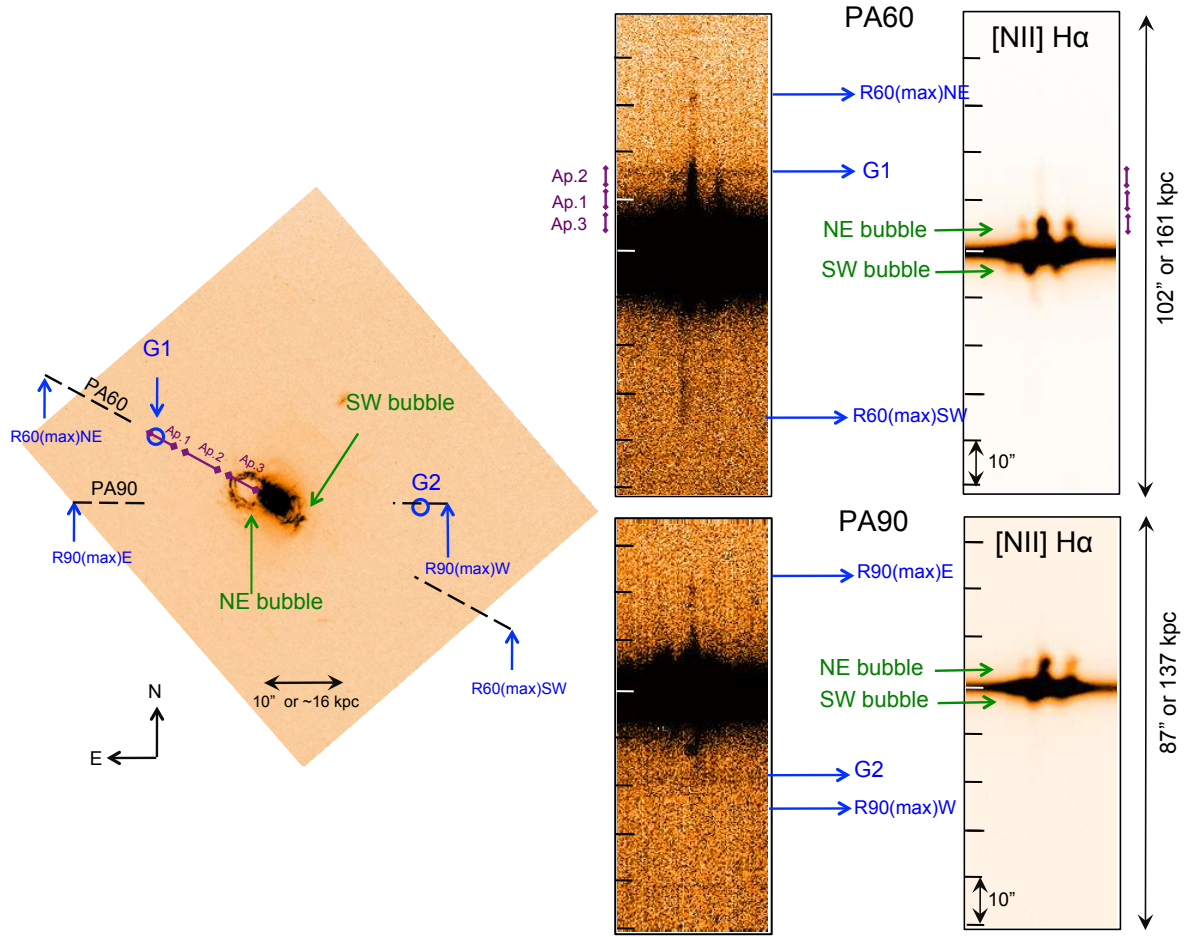


Figure 1. HST WFC3 FR716N image of the “Teacup” containing the $H\alpha$ + $[NII]$ lines. We highlight prominent emission line features such as the NE and SW bubbles. $R60(max)_{NE} \sim 53$ kpc, $R60(max)_{SW} \sim 58$ kpc, $R90(max)_E \sim 40$ kpc and $R90(max)_W \sim 31$ kpc are the maximum radial distances of the $H\alpha$ emission measured with the spectra along the PA60 and PA90 slits in directions NE, SW, E and W of the QSO2 nucleus respectively. The nebula is giant in comparison with the bubbles. The approximate location and size of apertures 1, 2 and 3 (Ap. 1, Ap. 2, Ap. 3) used to study the emission line spectra of the giant nebula and the NE bubble are also shown (see text). See the electronic edition for colour version of the figures.

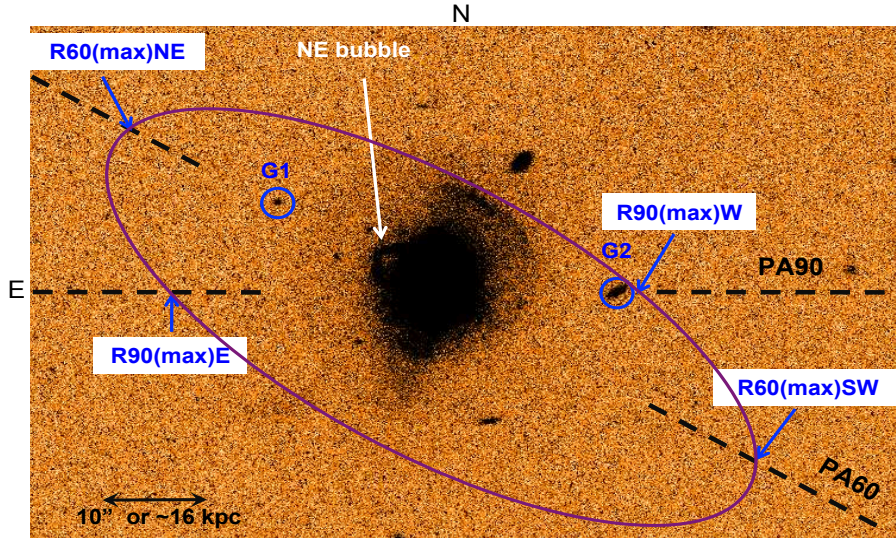


Figure 2. HST WFC3 F763M continuum image. We show again the striking dimensions of the giant gaseous reservoir around the Teacup. The purple elliptical area shows a possible geometry of the nebula (for instance, if settled in a rotating disk), adjusted in angle and size to fit the radial sizes of $H\alpha$ in different directions from the QSO2 along PA60 and PA90.

(Ap. 2) is centered at 16.6 arcsec (26.2 kpc) and is 3.6 arcsec wide (5.7 kpc). [NII] $\lambda\lambda 6548, 6583$, H α and [SII] $\lambda\lambda 6716, 6731$ are detected. [OI] $\lambda 6300$ is affected by a sky residual.

The [NII] $\lambda 6583$ /H α , [SII] $\lambda\lambda 6716, 6731$ /H α ratios and [OI] $\lambda 6300$ /H α upper limits are shown in Table 1 for both apertures. It is not possible to discriminate the ionization mechanism from these values alone (see Fig. 3). On the other hand, they are consistent with those measured by Gagne et al. (2014) for gas at numerous locations closer to the AGN, including different positions across the NE and SE bubbles (see Fig. 3, red ellipses). This suggests that the same ionizing mechanism excites the gas of the giant nebula. This mechanism is AGN photoionization (Gagne et al. 2014; see also Keel et al. 2017)

The [SII] doublet falls between two prominent sky emission lines so that sky residuals do not pose a problem to measure the doublet flux ratio. Using the Ap. 1 spectrum, for which the lines are stronger, we obtain $[SII]_{\lambda 6716/\lambda 6731} = 1.33 \pm 0.10$. Assuming an electron temperature in the range $T_e \sim 10,000$ - $20,000$ K, then $n \lesssim 240 \text{ cm}^{-3}$ (Osterbrock & Ferland 2006).

3.1.2 Kinematics of the giant nebula

We show in Fig. 4 the spatial variation of the FWHM (corrected for instrumental broadening) and the velocity shift V_s of H α relative to the nuclear emission line. The red shadowed areas mark the regions where contamination by the seeing smeared nuclear emission is expected to be significant relative to the extended emission (Villar Martín et al. 2016). Due to the complexity of the heavily blended nuclear [NII]+H α and the fact that we are mostly interested on the giant nebula and its properties in comparison with the bubbles, we do not show measurements within the inner areas where the emission is clearly dominated by the nucleus. The edges of the radio bubbles (Harrison et al. 2015) are marked with vertical black solid lines.

The H α kinematics become more quiescent at both sides of the AGN in the outer parts of the giant nebula. At $r > 12$ arcsec (19 kpc) the lines are narrower (in general unresolved with $\text{FWHM} \lesssim 150 \text{ km s}^{-1}$) and the V_s curve becomes almost flat. This is very clear along PA60 and can be hinted along PA90. At smaller radii, the lines are broader ($\text{FWHM} \sim \text{several} \times 100 \text{ km s}^{-1}$) and present a more complex velocity field with steep V_s profiles.

The kinematics of the gas within the bubbles have been studied by different authors. Gagne et al. (2014) proposed a rotational pattern dominating the motions within the inner ~ 5 arcsec with some disturbance possibly due to a merger. Small kinematic changes at the NE bubble edge (named “the handle” by the authors) also revealed the localized action of another mechanism that they propose to be an outflow. Other authors (Harrison et al. 2014, 2015, Keel et al. 2017, Ramos Almeida et al. 2017) have interpreted the motions in terms of the action of the giant outflow inflated by the AGN wind or the radio structures, acting across the whole volume covered by the expanding bubbles. Keel et al. (2017) claim that asymmetric [O III] profiles are present across the NE bubble, reaching maximum velocities of $\pm 1000 \text{ km s}^{-1}$. Ramos Almeida et al. (2017) also report tentative detection of a very broad Pa α component of $\text{FWHM} \sim 3000 \text{ km s}^{-1}$

at different locations across the bubbles. Such extreme kinematics would strongly support the outflow scenario.

We do not detect such extreme motions (neither do Harrison et al. 2015). We find turbulent gas (up to $\text{FWHM} \sim 450 \text{ km s}^{-1}$) across the bubbles (as found by Ramos Almeida et al. 2017 as well), but the kinematics are not extreme. We consider such FWHM values indicative of kinematic turbulence because even in the most dynamically disturbed mergers with signs of AGN activity, the extended non outflowing ionized gas shows typical $\text{FWHM} < 250 \text{ km s}^{-1}$ (Bellochi et al. 2013).

We also find that at the edges of both bubbles the gas presents the following kinematic changes compared with the gas within and beyond those locations (green arrows in Fig. 4): a) a clear broadening of the lines at the edge of SW bubble along PA60 (Fig. 4, top left panel), b) a clear broadening of the lines at the edge of the NE bubble to the E along PA90, c) a slight broadening of the lines at the edge of the NE bubble to the E (top right panel) and d) a slight change of V_s at the edge of the NE bubble along PA60 (bottom left panel). These results support that the expanding bubbles have an impact (at least local) on the underlying kinematic pattern.

However, a potential problem for the outflow scenario is that turbulent gas and prominent kinematic changes are also identified well beyond the bubble edges (blue arrows in Fig. 4). This is specially clear for gas beyond the SE bubble. At ~ 8 arcsec from the AGN along PA60 the line FWHM starts to increase sharply from $\sim 140 \text{ km s}^{-1}$ up to $\sim 350 \text{ km s}^{-1}$ at ~ 12 arcsec (Fig. 4, top left panel). This FWHM occurs far beyond the SW bubble edge, at ~ 6 arcsec or 9.5 kpc. Along PA90, at ~ 11 arcsec to the W the lines are significantly broader ($\text{FWHM} \sim 420 \text{ km s}^{-1}$) and much less blueshifted ($V_s \sim -20 \text{ km s}^{-1}$) than neighboring regions ($V_s \lesssim -145 \text{ km s}^{-1}$). This gas is ~ 4.7 arcsec or 7.4 kpc beyond the SW bubble edge. Such broad lines are rather extreme at such large distance from the galaxy nucleus (~ 19 kpc).

Therefore, turbulent gas exists far beyond the extension of the outflow traced by the bubbles. It is thus possible, that the gas motions within the inner ~ 12 arcsec are dominated by a mechanism other than the outflow, while this produces some localized perturbation at the edges of the expanding bubbles. It is not clear what that mechanism may be. The redistribution of gas by mergers/interactions may play a role. This is supported by the fact that the highest surface brightness stellar shells and tidal features seen in the continuum HST image (Fig. 2) are distributed within $r \lesssim 12$ arcsec from the AGN. However, as mentioned above, it is not clear that this mechanism alone can produce the large FWHM measured.

Alternatively, it is possible that the outflow reaches larger distances than mapped by the radio bubbles and/or that the effects from previous outflow episodes are still visible. This would not be surprising, since the radio emission shows mostly the working surface of the actual radio source, where the radio plasma currently interacts more strongly with the interstellar and/or intergalactic medium. Deeper or low frequency data may trace emission further out. Indeed, this is supported by the [OIII] $\lambda 5007$ morphology of Harrison et al. (2015) (see their Fig. 5), which shows faint ionized gas beyond the radio bubbles edges which and roughly circumscribing them.

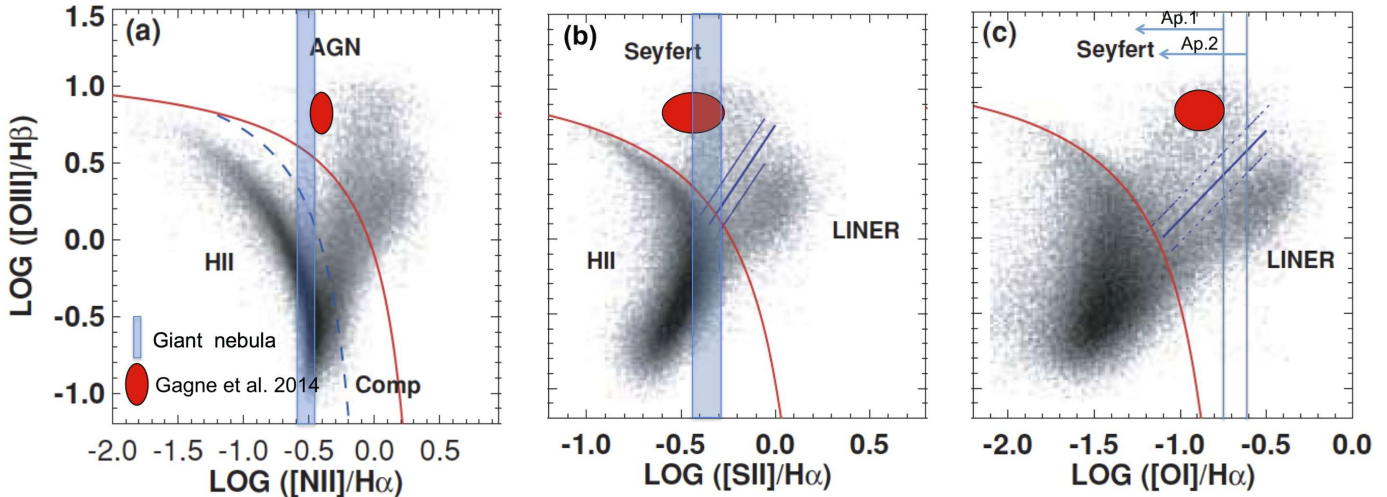


Figure 3. BPT (Baldwin et al. 1981) diagnostic diagrams taken from Kewley et al. (2006). Since the $[OIII]/H\beta$ ratio is not available for the “Teacup” nebula, only the location on the horizontal axis is constrained. The blue shadowed areas represent the range of values spanned by Ap. 1 and Ap. 2 (see text) including the uncertainties. It is not possible to discriminate the ionization mechanism from these line ratios alone. The red filled ellipses show the approximate area covered by the line ratios measured by Gagne et al. (2014) at different locations closer to the AGN, such as the NE and SW bubbles and the nucleus. The fact that the nebula presents line ratios that are consistent with those spanned by the red ellipses suggests that the same mechanisms (AGN photoionization) excites the gas.

Aperture	Distance to AGN kpc (NE)	Width kpc	$\frac{[NII]\lambda 6583}{H\alpha}$	$\frac{[OI]\lambda 6300}{H\alpha}$	$\frac{[SII]\lambda\lambda 6716,6731}{H\alpha}$
Ap. 1	18.2	7.6	0.31 ± 0.03	$\lesssim 0.18$	0.47 ± 0.04
Ap. 2	26.2	5.7	0.27 ± 0.03	$\lesssim 0.25$	0.40 ± 0.04

Table 1. Line ratios for apertures 1 and 2 (see text) along PA60 on the giant nebula at ~ 18 and ~ 26 kpc from the AGN well beyond the NE bubble. The width quoted in the 3rd column is the physical size of the apertures in kpc.

Therefore, there is not a definite explanation for the motions of the gas at $\lesssim 12$ arcsec from the AGN. A combination of the two mechanisms mentioned above may be at work. Disentangling this issue would be of great interest to understand the real impact of the radio or AGN induced outflow across its environment.

A relevant result is that the motions of the outer nebula ($\gtrsim 12$ arcsec) are detached from the kinematic pattern of the inner regions.

3.2 Coronal emission from the NE bubble

The kinematic, ionization, and morphological properties of the ionized bubbles (specially the NE one) have been studied in great detail in the literature (Keel et al. 2012,2015,2017, Gagne et al. 2014, Harrison et al. 2014,2015, Ramos Almeida et al. 2017). The new result we report here is the detection of coronal emission from the NE bubble.

We extracted a 1D spectrum of this region from an aperture selected to reach a compromise between S/N for the measurement of faint emission lines and minimizing the contamination from the QSO2 nuclear emission due to seeing smearing (Villar Martín et al. 2016). This aperture is centered at 5.7 arcsec (9.0 kpc) NE from the QSO2 continuum centroid along PA60 and is 3.8 arcsec (6.0 kpc) wide

(Ap. 3 in Fig. 1). Gagne et al. (2014) already showed that both the NE and SW bubbles emit rich emission line spectra. The larger aperture of the GTC has allowed to identify fainter lines undetected before (see Table 2 and Fig. 5), most interestingly, several coronal lines (CL) emitted by Fe^{+6} ($[FeVII]\lambda 5276, \lambda 5721$ and $\lambda 6086$). Based on the $[SiVI]\lambda 1.963 \mu m$ line, Ramos Almeida et al. (2017) confirmed the detection of an extended coronal outflow of size ~ 1 kpc almost coincident with the inner radio jet. The GTC spectrum shows that also the NE bubble emits CL, which therefore has a very broad range of ionization species, neutral (O^0), ionized (He^+ , H^+ , O^{+3} , etc) and coronal (Fe^{+6}). $[FeVII]\lambda 5721$ is detected also in the PA90 bubble spectrum. This shows that coronal emission occurs at different locations across the bubble.

The coronal lines are possibly blueshifted relative to lower ionization lines (Table 2), although they are faint and higher S/N spectra would be necessary to determine the precise redshift more accurately. If confirmed, this would reveal kinematic substructure in the bubbles dependent on the gas ionization level.

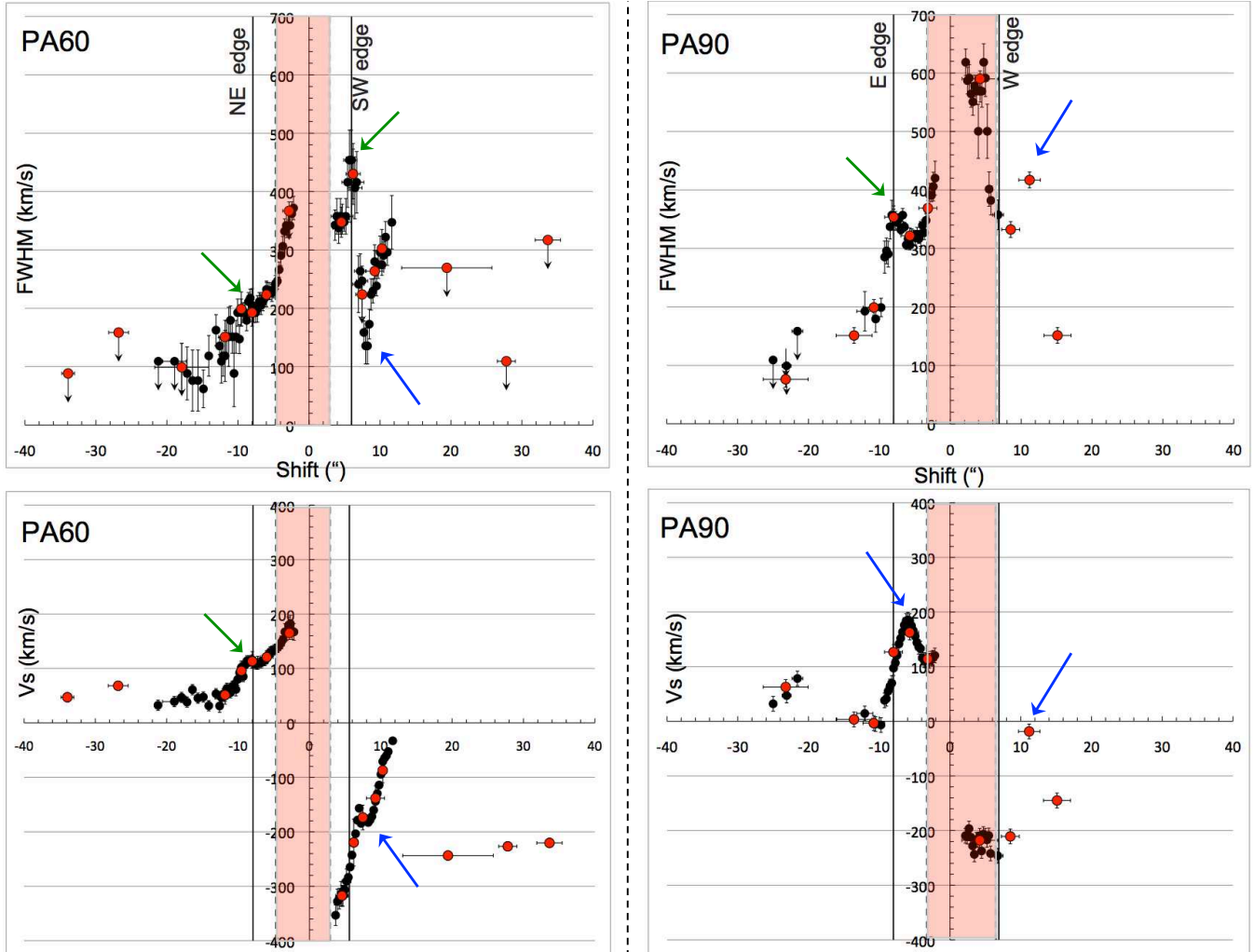


Figure 4. Kinematics of the extended gas along PA60 (left) and PA90 (right). The red shadowed areas indicate regions in which contamination by the nuclear emission is significant. The vertical black solid lines mark the approximate location of the edges of the radio bubbles (Harrison et al. 2015). Red solid circles correspond to measurements using larger apertures to increase the signal to noise ratio. The aperture sizes are indicated by the size of the horizontal bars. The green arrows mark kinematic changes identified at or very near the bubble edges. The blue arrows mark prominent kinematic changes not clearly associated with the bubbles.

4 DISCUSSION

4.1 The giant nebula

In the 1980’s and early 1990’s, long slit spectroscopy and narrow band emission line imaging revealed the existence of emission line gas with typical total sizes $D \lesssim$ several 10s of kpc in a significant fraction of radio loud quasars (Stockton & Mackenty 1987) and powerful radio galaxies with strong nuclear emission (e.g. Dazinger et al. 1984, Tadhunter et al. 1988, Baum et al. 1990). Different origins were proposed for the nebulae: tidal debris (remnants of galactic mergers/interactions), the optical signatures of cooling flows or gas swept out of the host galaxy by a large-solid-angle blast wave accompanying the production of the radio jets (Stockton & Mackenty 1987, Baum et al. 1992, Fu & Stockton 2009). More recent studies have revealed that also radio quiet quasars are associated with extended ionized nebulae (Liu et al. 2013, Harrison et al. 2014, Humphrey et al. 2015, Villar Martín et al. 2016) with typical total extensions

also $D \lesssim$ several 10s kpc although it appears that they are frequently smaller than those around radio loud systems.

Some ionized nebulae are giant, although $D \gtrsim 100$ kpc are rare and very extreme at low z . Among the largest around active galaxies at $z \lesssim 0.4$ are those associated with³:

- the radio galaxies PKS 0349-27 ($z=0.066$, $D \sim 60$ kpc, Danziger et al. 1984), 3C227 ($z=0.086$, $D \sim 111$ kpc, Prieto et al. 1993), Coma A ($z=0.086$, $D \sim 70$ kpc, van Breugel et al. 1985, Tadhunter et al. 2000), PKS 1932-464 ($z=0.230$, $D \sim 145$ kpc, Villar Martín et al. 2005)

- the radio loud type 1 quasars 4C37.43 ($z=0.370$, $D \sim 140$ kpc, Stockton et al. 2002), 3CR249.1 ($z=0.312$, $D \sim 67$ kpc, Stockton & MacKenty 1983), the radio quiet type 1 quasar MR 2251-178 ($z=0.064$, $D \sim 200$ kpc, Shopbell et al. 1999)

³ The sizes have been converted to the same cosmology used in this work

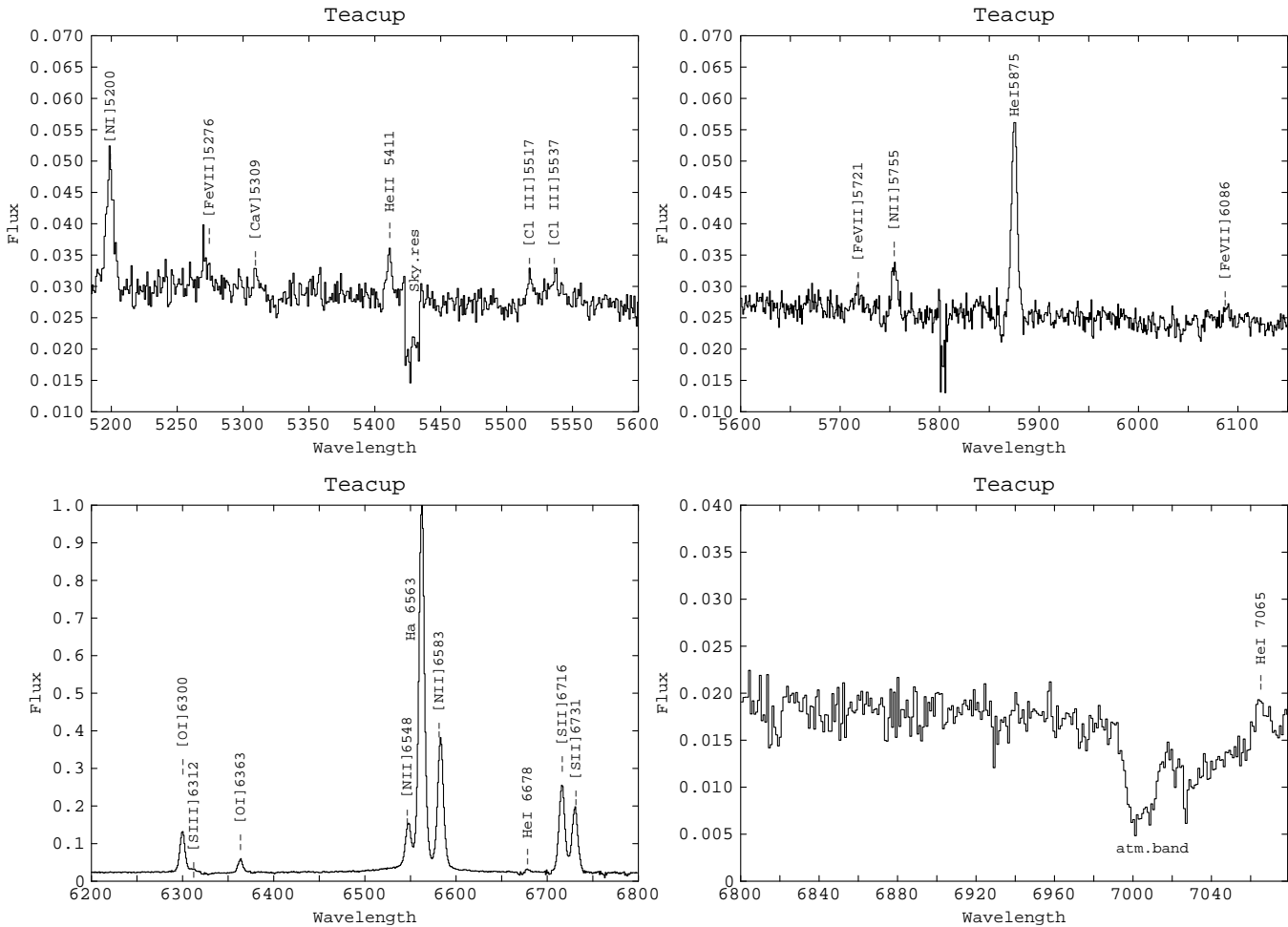


Figure 5. Spectrum of the NE bubble split in four spectral windows with different flux scales to highlight some of the weakest lines. Wavelength (rest-frame) in Å. The flux in all spectra has been normalized to the peak of H α . Several coronal lines are detected: [FeVII] λ 5276, λ 5721, λ 6086.

- the radio quiet type 2 quasars SDSS J0123+10 ($z=0.399$, $D \sim 180$ kpc, Villar Martín et al. 2010), SDSS J1356+1026 ($z=0.123$, $D \sim 80$ kpc, Greene et al. 2012) and SDSS J1653+23, nicknamed the “Beetle” ($z=0.103$, $D \sim 70$ kpc, Villar Martín et al. 2017)

The excitation of the gas is always related at least partially to AGN photoionization. Stellar photoionization has also been identified in some of these giant nebulae (e.g. Villar Martín et al. 2005,2010).

Giant extensions appear more common in the high z Universe ($z \gtrsim 2$), where $\gtrsim 100$ kpc Ly α nebulae are sometimes found associated with radio loud AGN, both quasars and radio galaxies (McCarthy et al. 1993, Heckman et al. 1991, Villar Martín 2007), radio quiet AGN (Borisova et al. 2016) and with (apparently) non active galaxies (Chapman et al. 2001, Matsuda et al. 2011). A selection effect is possibly at work, since more luminous AGN can in principle ionize gas at larger distances. It is also possible that higher z AGN are immersed in larger gaseous reservoirs.

The nebula we have discovered associated with the “Teacup” is among the largest known at any z , specially at $z \lesssim 0.4$. It has two things in common with the low z AGN with reported giant nebulae: they are very luminous

active galaxies and they show clear signs of past or ongoing galactic interactions, with rich tidal features of different morphologies (shells, tails, bridges, etc). This is consistent with Stockton & MacKenty (2002), who found a correspondence between the incidence of strong extended ionized nebulae among type 1 quasars and the presence of overt signs of strong galactic interactions, such as close companion galaxies and continuum tails or bridges.

Large-scale (up to almost ~ 200 kpc) neutral hydrogen HI structures have been detected around several low z radio galaxies (Morganti et al. 2002a,2002b, Emonts et al. 2010; see also Oosterloo et al. 2010) in emission or in absorption against the radio lobes. They sometimes consist of enormous rotating discs/rings of HI gas, probably resulting from the merger of gas rich galaxies.

All these giant reservoirs of neutral and ionized gas may be the manifestation of the same phenomenon: galactic interactions populate the circumgalactic medium (CGM) with tidal debris, which sometimes are photoionized and rendered visible thanks to the illumination by the active nucleus. We thus propose that the “Teacup” giant nebula is part of the CGM. The optical/radio bubbles, which are comparatively very small, appear to be expanding across this medium. This

(1) Species	(2) λ_{air} (Å)	(3) λ_{obs} (Å)	(4) $\Delta(V)$ km s ⁻¹	(5) $100 \times \frac{\text{Flux}}{\text{Flux}(H\alpha)}$
[NI]	5197.9+5200.4	5643.9±0.5	-24±24	1.88±0.02
[Fe VII]*	5276.4	5724.1±0.7	-197±28	0.50±0.05
[CaV]	5309.1	5764.5±0.6	60±28	0.32±0.06
HeII	5411.5	5874.5±0.2	0±15	0.67±0.07
[Cl III]	5517.7	5990.7±0.4	44±21	0.36±0.08
[Cl III]	5537.9	6011.0±1.0	-37±44	0.37±0.08
[FeVII]	5720.9	6207.4±0.5	-134±24	0.38±0.10
[NII]	5754.6	6247.6±0.2	32±14	0.83±0.05
HeI	5875.6	6378.4±0.2	3±15	3.2±0.03
[FeVII]	6086.9	6607.1±1.8	-28±77	0.32±0.04
[OI]	6300.3	6839.4±0.2	1±15	10.1±0.2
[SIII]	6312.1	6851.0±0.3	-53±17	1.10±0.04
[OI]	6363.8	6908.5±0.2	7±15	2.89±0.13
[NII]	6548.1	7108.7±0.2	14±15	12.4±1.5
H α	6562.8	7124.3±0.2	0±12	100.0
[NII]	6583.5	7146.8±0.2	-2±15	36.3±2.6
HeI	6678.2	7249.7±0.8	4±36	0.92±0.07
[SII]	6716.4	7291.2±0.2	5±15	25.0±0.7
[SII]	6730.8	7306.7±0.2	6±15	18.8±0.2
HeI	7065.7	7670.6±0.5	13±23	0.40±0.13

Table 2. Emission lines identified in the spectrum of the NE bubble. Columns (2) and (3) give the rest frame and observed λ . $\Delta(V)$ in (4) is the shift in velocity relative to H α . The line ratios in (5) are given relative to H α , with $F(H\alpha)=(7.60\pm0.06)\times10^{-15}$ erg s⁻¹ cm⁻². *Contamination of [Fe VII] λ 5276.4 by [Fe III] and [FeII] lines is expected to be negligible, given the non detection of other lines by the same species (see Villar Martín et al. 2015).

is suggested by the observed impact on the global kinematic pattern in at least some localized positions near or at the bubble edges.

Some of the gaseous reservoirs mentioned above have had enough time to settle in giant rotating disks or rings. The quiescent kinematics of the “Teacup” outer nebula is indeed reminiscent of rotation, although integral field spectroscopy would be required to constraint the 2D velocity pattern more accurately. If the giant nebula is settled in a disk with rotational velocity V_{rot} , we can estimate the dynamical mass contained within its radius $R \sim 50$ kpc, via:

$$M_{\text{dyn}}(r < R) \approx \frac{(V_{\text{obs}}/\sin(i))^2 R}{G}$$

where i is the inclination relative to the plane of the sky ($i=90^\circ$, edge on), $V_{\text{rot}} = \frac{V_{\text{obs}}}{\sin(i)}$, $V_{\text{obs}} \sim 150$ km s⁻¹ is half the amplitude of the observed rotation curve, as inferred from Fig. 4 and G is the gravitational constant. We have constrained $i \sim 70^\circ$ very roughly using Fig. 2. This implies $M_{\text{dyn}} \sim 3.0 \times 10^{11} M_\odot$. For comparison, the total stellar mass of the “Teacup” host galaxy is $M_{\text{stars}} \sim 6.3 \times 10^{10} M_\odot$ according to the Vizier catalogue (Ochsenbein et al. 2000) based on Mendel et al. (2014). Taking into account dark matter, the total mass is probably a few times higher (Nigoche-Netro et al. 2016). Therefore, although these calculations are based on strong assumptions, in principle the total mass of the “Teacup” host galaxy appears sufficient to sustain the rotation of the giant nebula.

The emission line spectrum of the giant nebula demonstrates that the AGN can ionize gas at huge distances (>50 kpc) well beyond the optical size of the host galaxy (Sect. 3.1.1). Therefore, unless some unknown mechanism protects

the molecular reservoir or this is accumulated mostly in a location protected from the hard ionizing continuum, the quasar can transform the environment within a huge volume into a very hostile environment for star formation. It would be interesting to investigate whether this mechanism can explain some of the fundamental issues related to the formation and evolution of massive galaxies that the community are trying to solve with powerful AGN driven winds (e.g. Silk & Rees 1998, King 2003, di Matteo et al. 2005). Is it possible that the harsh effects of the illumination by active nuclei are enough to quench star formation in the amount we need to solve those fundamental issues?

The CGM is the scene where large scale inflow and outflow from galaxies takes place. The competition between these processes is thought to shape galaxies and drive their evolution. Therefore, detailed studies of the giant nebulae associated with luminous AGN may probe to be useful to trace back their formation and evolution history. The presence of a luminous AGN can render visible the CGM gas around active galaxies which otherwise may not be detected or only via absorption line studies.

4.2 The ionization mechanism and the fading of the AGN

We investigate next whether the AGN can provide sufficient photons to explain the line ratios of the giant nebula. For this we follow Gagne et al. (2014) using our own photoionization models.

We use the definition of the ionization parameter $U = \frac{Q(H^0)}{4\pi r^2 n c}$, where n is the gas density, c is the speed of light, $Q(H^0)$ is the ionizing luminosity emitted by the AGN in photons s⁻¹ and r is the distance in cm from

the ionized clouds to the AGN. U will be constrained with the photoionization models, which together with r and n , will provide $Q(H^0)$. Because we have very limited information to constrain the models (only $[\text{NII}]\lambda 6583/\text{H}\alpha$, $[\text{SII}]\lambda\lambda 6716, 6731/\text{H}\alpha$ and upper limits on $[\text{OI}]\lambda 6300/\text{H}\alpha$, Sect. 3.1.1), our goal is to obtain an approximate U value. We will then test our results comparing with Gagne et al. (2014) method and results.

We have used sequences of photoionization models built with the code MAPPINGS1e (Binette et al. 1985, Ferruit et al. 1997) as described in Silva et al. (2017) (see also Humphrey et al. 2008). The metallicity Z ranges from $0.5Z_\odot$ to $2Z_\odot$ in steps of 0.1; the ionization parameter U ranges from 0.0001 to 1.6 in steps of 0.002. A power law of index α is assumed for the ionizing continuum. Two α values were considered, -1.0 and -1.5 with high-energy cut-offs of 10^3 eV and 5×10^4 eV respectively. For all models, the gas density is $n = 100 \text{ cm}^{-3}$. The predicted line ratios were compared with the observed ones and the best model was selected using the reduced chi-square (χ^2_ν).

Given the similar line ratios of Ap. 1 and Ap. 2, the same optimum model is selected for both. If solar abundances $Z = Z_\odot$ are considered (as Gagne et al. 2014), the best model has $\alpha = -1.5$ and $U = 0.003$ (see Table 3, Model I). For the assumed ionizing continuum, $\frac{Q_{H^0}}{L_{\text{ion}}} \sim 1.6 \times 10^{10}$, where L_{ion} is the ionizing luminosity in erg s^{-1} . Assuming $L_{\text{ion}} = 0.35 \times L_{\text{bol}}$ (Stern et al. 2014) we can now infer the bolometric luminosity seen by the gas at the corresponding distances of Ap. 1 and 2. We obtain $\log(L_{\text{bol}}) = 46.80$ for Ap. 1 and 47.11 for Ap. 2. These are ~ 280 and ~ 575 times higher than $\log(L_{\text{bol}}) = 44.36$ inferred by Gagne et al. (2014) at the nucleus⁴.

As a test, we have also constrained L_{bol} based on the more sophisticated AGN photoionization models presented by Gagne et al. (2014), who also assumed solar abundances. We have identified in their Table 4 locations across the bubbles with line ratios as similar as possible to Ap. 1. and Ap. 2 of the giant nebula (e.g. positions (4”, 0”) and (-2”, 4”) using their system of coordinates). We have then used the U and n values of the optimum models selected by these authors for these locations: $\log(U_{\text{high}}) = -2.4$, $\log(n_{\text{high}}) = 2.1$; $\log(U_{\text{low}}) = -3.2$, $\log(n_{\text{low}}) = 2.9$; see their Table 5). Using the appropriate distances we now infer as above $\log(L_{\text{bol}}) \sim 46.96$ for Ap. 1 and 47.28 for Ap. 2, which are in good agreement with our values.

We find that subsolar abundances ($Z = 0.5Z_\odot$) result on a better agreement between the observed and theoretical ratios⁵. Our best model has $\alpha = -1.5$, $Z = 0.5Z_\odot$ and $U = 0.0006$ (Table 3, Model II). In this case, $\log(L_{\text{bol}}) = 46.11$ for Ap. 1 and 46.42 for Ap. 2, which are ~ 56 and ~ 115 times higher than L_{bol} seen by the nuclear gas.

Clearly, the effect of the metallicity on the inferred L_{bol} is important, but both models (Z_\odot and $0.5Z_\odot$) imply that

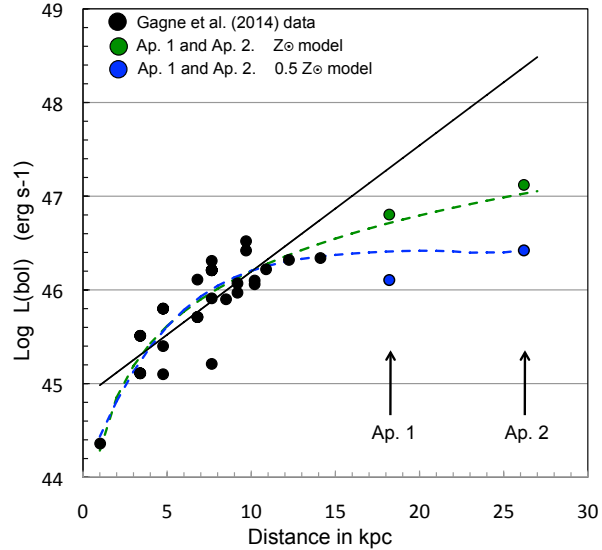


Figure 6. Fading of the AGN. Log of bolometric luminosity for the ionized gas at different locations plotted relative to the projected distance from the AGN. This figure is based on Fig. 11 of Gagne et al. (2014). Ap. 1 and Ap. 2 of the giant nebula are added. The two L_{bol} values shown for each aperture correspond to the predicted values for our Z_\odot (green) and $0.5Z_\odot$ (blue) photoionization models. The linear fit obtained by Gagne et al. (2014) is shown in black. The new fits implied by the addition of the giant nebula Ap. 1 and Ap. 2 are shown in green and blue. The emission line ratios of the nebula imply that the AGN was more luminous in the past and thus support the quasar fading scenario.

the L_{bol} seen by the giant envelope is significantly larger than that seen by gas closer to AGN.

Robinson et al. (2000) found a related discrepancy for the radio galaxy 3C321. They showed that the remarkable constancy of the optical line ratios across different spatial regions implies a bolometric luminosity significantly higher than that inferred for the AGN, if the extended ionized medium consists of an ensemble of ionization bounded clouds. The alternative solution they propose is that this medium consists instead of a mixture of optically thin and thick clouds illuminated by a power-law continuum.

Gagne et al. (2014) propose a different scenario (see also Keel et al. 2017). These authors inferred the L_{bol} implied by the line ratios measured at multiple locations across the “Teacup” NW and SW bubbles. They found that the L_{bol} seen by the gas decreases with decreasing distance to the nucleus, with a drop of more than two orders of magnitude from ~ 15 kpc to the AGN. They conclude that the active nucleus has decreased in luminosity in a continuous fashion over $\sim 46,000$ yr.

Our results are consistent with this scenario and support that the “Teacup” quasar was more luminous in the past. We show in Fig. 6 the L_{bol} seen by the gas at increasing distances from the AGN, based in Fig. 11 of Gagne et al. (2014). Both the solar and specially the subsolar abundance models imply that the L_{bol} vs. r curve flattens at increasing distances. This suggests that the dimming rate has not been constant with time. Depending on the true abundance, the conclusions are different. The Z_\odot model suggests that the

⁴ Harrison et al. (2015) infer $\log(L_{\text{bol}}) = 45.3$ derived from the midfar-infrared spectral energy distribution. We use Gagne et al. (2014) value for a more consistent comparison with their method and results.

⁵ Keel et al. (2017) inferred slightly subsolar abundances for the bubbles

(1) Ratio	(2) Ap .1 18.2 kpc	(3) Ap. 2 26.2 kpc	(4) Model I $\alpha=-1.5, n=100 \text{ cm}^{-3}$ $Z_{\odot}, U=0.003$	(5) Model II $\alpha=-1.5, n=100 \text{ cm}^{-3}$ $0.5Z_{\odot}, U=0.0006$
$\frac{[NII]\lambda 6583}{H\alpha}$	0.31±0.03	0.27±0.03	0.36	0.29
$\frac{[OII]\lambda 6300}{H\alpha}$	≲0.18	≲0.25	0.20	0.23
$\frac{[SII]\lambda\lambda 6716,6731}{H\alpha}$	0.47±0.04	0.40±0.04	0.28	0.44
$\log(L_{\text{bol}})$ Ap. 1			46.80	46.11
$\log(L_{\text{bol}})$ Ap. 2			47.11	46.42

Table 3. Measured line ratios (columns 2 and 3) for apertures Ap. 1 and Ap. 2. Columns (4) and (5) show the predicted ratios for the optimum AGN photoionization models with solar (4) and half solar (5) abundances. The $0.5Z_{\odot}$ model reproduces the measured ratios better. The two bottom lines show the bolometric luminosities (log) in erg s^{-1} seen by the gas at the distances of Ap. 1 and 2 implied by the U values of the photoionization models.

fading of the AGN was slower in the past. It has occurred for $\sim 86,000$ yr during which the AGN luminosity has dropped by ~ 575 times⁶. If the giant nebula has subsolar abundances, the dimming started $\sim 46,000$ yr ago during which the AGN faded ~ 100 times (Gagne et al. 2014).

Deep wide field integral field spectroscopy of the giant nebula covering a broad spectral range would be extremely valuable to advance in this study. More optical line ratios (including the critically important $[OIII]\lambda 5007/H\beta$) measured across the extension of the nebula, up to the measured $R_{\text{max}} \sim 50$ kpc, would allow to constrain more accurately the abundance and U values at different locations. This is essential to characterize more precisely the temporal variation of the “Teacup” bolometric luminosity.

4.3 Coronal emission from the NE bubble

In general, the coronal emission in active galaxies is concentrated within small distances from the AGN, extending from just a few parsecs up to 230 pc. This is consistent with the bulk of the coronal lines (CLs) originating between the broad-line region (BLR) and the NLR, and extending into the NLR in the case of Fe^{+6} and Ne^{+4} lines (e.g. Mazzalay et al. 2010). They are believed to be excited by AGN photoionization (e.g. Mazzalay et al. 2010). Objects showing coronal emission at such large distances as the “Teacup” (~ 10 kpc) are very rare. Another example is the radio galaxy PKS 2152-69 at $z = 0.028$ (Tadhunter et al. 1988). A luminous cloud located at ~ 11 kpc from the nucleus emits CLs, including $[\text{FeX}]\lambda 6374$.

The detection of $[\text{FeVII}]$ emission along PA60 and PA90 suggests that the mechanism exciting the coronal lines acts across a large volume of the NE bubble. This is against a scenario such that a highly collimated radio jet excites the lines locally as it interacts with the gas in its advance through the ambient medium (Tadhunter et al. 1988).

Based on theoretical arguments, Ferguson et al. (1997) showed that CLs form at distances from just outside the BLR (the highest ionization lines) up to a maximum distance $R_{\text{CL}} \sim 400L_{43.5}^{1/2}$ pc (the lowest ionization lines, such as

those emitted by Fe^{+6}). $L_{43.5}$ is the ionizing luminosity in units of $10^{43.5} \text{ erg s}^{-1}$. This upper limit could be higher for gas densities $< 100 \text{ cm}^{-3}$.

Our measured $R_{\text{CL}} \sim 9.0$ kpc requires $L_{43.5} \sim 506$ and this implies $\log(L_{\text{bol}}) \sim 46.7$. Gagne et al. (2014) concluded that the emission line spectrum at this same distance implies $\log(L_{\text{bol}}) \sim 46.0 \pm 0.2$, which is remarkably similar, taking into account all possible uncertainties (uncertainty on R_{CL} , scatter of the relations L_{bol} vs. Distance for the “Teacup”, L_{bol} vs. L_{ion} and R_{CL} vs. $L_{43.5}$). For comparison, $R_{\text{CL}} \sim 640$ pc is inferred for the current $\log(L_{\text{bol}}) = 44.36$ implied by the nuclear spectrum. It thus appears feasible that the large size of the coronal region is consistent with photoionization by the central AGN, provided it was brighter in the past, in consistency with the fading quasar scenario.

5 SUMMARY AND CONCLUSIONS

We present new results on the radio quiet type 2 quasar (QSO2) nicknamed the “Teacup” ($z=0.085$) based on long slit spectroscopic data obtained with the 10.4m Gran Telescopio Canarias (GTC). We have discovered that the QSO2 is associated with a giant reservoir of ionized gas which extends across ~ 111 kpc along PA60 and at least 71 kpc along PA90. It is among the largest known ionized nebulae associated with active galaxies at any z . The well known radio/optical bubbles (~ 10 - 12 kpc in size) are comparatively tiny.

We propose that the giant nebula is part of the circumgalactic medium of the “Teacup”, which has been populated with tidal debris (maybe settled in a giant rotating disk) by galactic interactions. This rich gaseous medium has been rendered visible due to the illumination by the powerful active nucleus. The optical/radio bubbles appear to be expanding across this medium, given their impact on the global kinematic pattern in at least some localized positions.

The kinematics of the nebula are much more quiescent (very narrow lines $\text{FWHM} \lesssim 150 \text{ km s}^{-1}$, flat velocity field at both sides of the AGN) in the outer parts at $\gtrsim 20$ kpc from the AGN. The more chaotic motions at smaller radii reveal a different mechanism affecting the kinematics that is in part (possibly not only) related to the radio/optical bubbles.

The nebula is most likely photoionized by the AGN. Subsolar abundances ($\sim 0.5Z_{\odot}$) are suggested by the optical

⁶ The recombination ($\sim \frac{10^5}{n_e}$ yr) and cooling ($\sim \frac{10^4}{n_e}$ yr) times, where n_e is the electron density in cm^{-3} , are short compared to the light-travel times (Osterbrock & Ferland 2006).

line ratios, although a broader spectral coverage would help to constrain the metallicity more accurately. Its emission line spectrum implies that the active nucleus was more luminous in the past, in consistency with the fading quasar scenario suggested by Gagne et al. (2014). Depending on the nebular abundances, the conclusions are different regarding the temporal variation of the AGN luminosity. The Z_{\odot} model suggests that the dimming of the AGN was slower in the past. It has occurred for $\sim 86,000$ yr during which the AGN luminosity has dropped by ~ 575 times. The subsolar abundance model suggests that the dimming started $\sim 46,000$ yr ago and the AGN has faded a factor of ~ 115 since.

We also report the detection of coronal emission (Fe^{+6}) from the NE bubble, at ~ 9 kpc from the AGN. The detection of coronal lines at such large distances is very infrequent. For the “Teacup” it can be explained by AGN photoionization, provided the QSO2 was much more luminous in the past. This adds further support to the fading quasar scenario.

The CGM is the scene where large scale inflow and outflow from galaxies takes place. The competition between these processes is thought to shape galaxies and drive their evolution. Deep wide field integral field spectroscopy of powerful AGN with instruments such as MUSE on VLT opens up a way to detect and study the elusive material from the CGM around massive active galaxies thanks to the presence of a luminous AGN that can render it visible.

ACKNOWLEDGMENTS

We thank the referee William Keel for interesting scientific suggestions.

This work is based on observations carried out at the Observatorio Roque de los Muchachos (La Palma, Spain) with GTC (programme GTC13-16B). We thank the GTC staff for their support with the observations. MVM and ACL acknowledge support from the Spanish Ministerio de Economía y Competitividad through the grant AYA2015-64346-C2-2-P.

The National Radio Astronomy Observatory is a facility of the National Science Foundation operated under cooperative agreement by Associated Universities, Inc.

This research has made use of 1) the VizieR catalogue access tool, CDS, Strasbourg, France. The original description of the VizieR service was published in Ochsenein et al. A&AS, 143, 23; 2) the NASA/IPAC circumgalactic Database (NED) which is operated by the Jet Propulsion Laboratory, California Institute of Technology, under contract with the National Aeronautics and Space Administration.

REFERENCES

- Baldwin J. A., Phillips M. M., Terlevich R., 1981, PASP, 83, 5
- Barnes J., 2002, MNRAS, 333, 481
- Baum S., Heckman T., van Breugel W., 1990, ApJS, 74, 389
- Baum S., Heckman T., van Breugel W., 1992, ApJ, 389, 208
- Borisova E., Cantalupo S., Lilly S.J. et al., 2016, ApJ, 831, 39
- Bellocchi E., Arribas S., Colina L., Miralles-Caballero D., 2013, A&A, 557, 59
- Binette L., Dopita M. A., Tuohy I. R., 1985, ApJ, 297, 476
- Chapman S.C., Lewis G.F., Scott D., Richards E., Borys C., Steidel C.C., Adelberger K.L., Shapley A.E., 2001, ApJ, 548, L17
- Danziger I.J., Fosbury R.A.E., Goss W.M., Bland J., Boksenberg A., 1984, MNRAS, 208, 569
- Di Matteo T., Springel V., Hernquist L., 2005, Nature, 433, 604
- Emonts B.H.C. et al. 2010, MNRAS, 406, 987
- Ferguson J.W., Korista K.T., Ferland G., 1997, ApJS, 110, 287
- Ferruit P., Binette L., Sutherland R. S., Pecontal E., 1997, A&A, 322, 73
- Fu H., Stockton A., 2009, ApJ, 690, 953
- Gagne J. P., Crenshaw, D. M., Kraemer, S. B. et al., 2014, ApJ, 792, 72
- Greene J.E., Zakamska N.L., Smith P. S., 2012, ApJ, 746, 86
- Harrison C. M., Alexander D. M., Mullaney J. R., Swinbank A. M., 2014, MNRAS, 441, 3306
- Harrison C. M., Thomson A.P., Alexander D. M., Bauer F.E., Edge A.C., Hogan M.T., Mullaney J. R., Swinbank A. M., 2015, ApJ, 800, 45
- Heckman T., Lehnert M., van Breugel W., Miley G., 1991, ApJ, 370, 78
- Humphrey A., Villar Martín M., Vernet J., Fosbury R., di Serego Alighieri S., Binette L., 2008, MNRAS, 383, 11
- Humphrey A., Villar Martín M., Ramos Almeida C., Tadhunter C. N., Arribas S., Bessiere P.S., Cabrera-Lavers A., 2015, MNRAS, 454, 4452
- Keel W.C., Chojnowski S.D., Bennert V. N., 2012, AJ, 420, 878
- Keel W.C., Maksym W.P., Bennert V.N. et al., 2015, AJ, 149, 155
- Keel W.C., Linlott C.J., Maksym W.P. et al. 2017, ApJ, 835, 256
- Kewley L., Groves B., Kauffmann G., Heckman T., 2006, MNRAS, 372, 961
- King A., 2003, ApJ, 596, L27
- Liu G., Zakamska N., Greene J., Nesvadba N., Liu X., 2013, MNRAS, 430, 2327
- Silva M., Humphrey A., Lagos P., Villar Martín M., Morais S., di Serego Alighieri S., Cimatti A., 2017, MNRAS, submitted
- Matsuda Y., Yamada T., Hayashino T. et al. 2011, MNRAS, 410, 13
- Mazzalay X., Rodríguez-Ardila A., Komossa S., 2010, MNRAS, 405, 1315
- McCarthy P.J., 1993, ARA&A, 31, 639
- Mendel J. T., Simard L., Palmer M., Ellison S. Patton D., 2014, ApJS, 210, 3
- Morganti R., Oosterloo T. A., Tinti S., Tadhunter C. N., Wills K. A., van Moorsel G., 2002a, A&A, 383, 830
- Morganti R., Oosterloo T. A., Tinti S., Tadhunter C. N., Wills K. A., van Moorsel G., 2002b, in *Seeing Through the Dust: The Detection of HI and the Exploration of the ISM in Galaxies*, ASP Conference Proceedings, Eds. A. R. Taylor, T. L. Landecker, and A. G. Willis. Vol. 276, p.

423. ISBN: 1-58381-118-4.
- Nigoche-Netro A. et al. 2016, MNRAS, 462, 951
- Ochsenbein F., Bauer P., Marcout J., 2000, A&AS, 143, 23
- Oosterloo T. et al, 2010, MNRAS, 409, 500
- Osterbrock D.E., Ferland G.J., 2006, *Astrophysics of Gaseous Nebulae and Active Galactic Nuclei*. University Science Books. ISBN 1891389343
- Prieto M.A., Walsh J.R., Fosbury R.A.E., di Serego Alighieri S., 1993, MNRAS, 263, 10
- Ramos Almeida C., Piqueras J., Villar Martín M., Bessiere P., 2017, MNRAS, 470, 964
- Robinson T.G., Tadhunter C.N., Axon D.J., Robinson A., 2000, MNRAS, 317, 922
- Shopbell P.L., Veilleux S., Bland-Hawthorn J., 1999, ApJL, 524, 83
- Silk J., Rees M., 1998, A&A, 331, L1
- Stern J., Laor A., Baskin A., 2014, MNRAS, 438, 901
- Stockton A., MacKenty J. W., 1983, Nature, 305, 678
- Stockton A., MacKenty J. W., 1987, ApJ, 316, 584
- Stockton A., MacKenty J. W., Hu M.H., Kim T.H., 2002, ApJ, 572, 735
- Tadhunter C. N., Fosbury R. A. E., di Serego Alighieri S., Bland J., Danziger I. J., Goss W. M., McAdam W. B., Snijders M. A. J., 1988, MNRAS, 235, 403
- Tadhunter, C. N., Villar-Martin M., Morganti R., Bland-Hawthorn J., Axon D., 2000, MNRAS, 314, 849
- van Breugel W., Miley G., Heckman T., Butcher H., Bridle A., 1985, ApJ, 290, 496
- Villar Marín M., Tadhunter C., Morganti R., Holt J., 2005, MNRAS, 359, L5
- Villar Martín M., 2007, NewAR, 51,194
- Villar Martín M., Tadhunter C., Pérez E., Humphrey A., Martínez-Sansigre A., González Delgado R., Pérez Torres M., 2010, MNRAS, 407, L6
- Villar Martín M., Bellocchi E., Stern J., Ramos Almeida C., Tadhunter C., González Delgado R., 2015, MNRAS, 454, 439
- Villar Martín M., Arribas S., Emonts B., Humphrey A., Tadhunter C., Bessiere P., Cabrera Lavers A., Ramos Almeida C., 2016, MNRAS, 460, 130
- Villar Martín M., Emonts B., Cabrera Lavers A. et al. 2017, MNRAS, in press (arXiv:1708.07530)